

The Power Spectrum of Rich Clusters of Galaxies on Large Spatial Scales

Helen Tadros¹, George Efstathiou², and Gavin Dalton².

¹*Astronomy Centre, University of Sussex, Falmer, Brighton BN1 9QH, U.K.*

²*Department of Physics, University of Oxford, Keble Road, Oxford, OX1 3RH, UK.*

11 October 2021

ABSTRACT

We present an analysis of the redshift-space power spectrum, $P(k)$, of rich clusters of galaxies based on an automated cluster catalogue selected from the APM Galaxy Survey. We find that $P(k)$ can be approximated by a power law, $P(k) \propto k^n$, with $n \approx -1.6$ over the wavenumber range $0.04 \text{ h Mpc}^{-1} < k < 0.1 \text{ h Mpc}^{-1}$. Over this range of wavenumbers, the APM cluster power spectrum has the same shape as the power spectra measured for optical and IRAS galaxies. This is consistent with a simple linear bias model in which different tracers have the same power spectrum as that of the mass distribution but shifted in amplitude by a constant biasing factor. On larger scales, the power spectrum of APM clusters flattens and appears to turn over on a scale $k \sim 0.03 \text{ h Mpc}^{-1}$. We compare the power spectra estimated from simulated APM cluster catalogues to those estimated directly from cubical N-body simulation volumes and find that the APM cluster survey should give reliable estimates of the true power spectrum at wavenumbers $k \gtrsim 0.02 \text{ h Mpc}^{-1}$. These results suggest that the observed turn-over in the power spectrum may be a real feature of the cluster distribution and that we have detected the transition to a near scale-invariant power spectrum implied by observations of anisotropies in the cosmic microwave background radiation. The scale of the turn-over in the cluster power spectrum is in good agreement with the scale of the turn-over observed in the power spectrum of APM galaxies.

Key words: cosmology: large-scale structure of Universe

1 INTRODUCTION

Most modern theories of structure formation, including those based on inflation or topological defects in the early Universe, predict a near scale-invariant spectrum of density perturbations on large spatial scales. On small spatial scales, $\lambda \lesssim 10 \text{ h}^{-1}\text{Mpc}$, the observed fluctuations in the galaxy distribution differ very substantially from a scale-invariant form. For example, the power spectra estimated from infra-red and optically selected redshift surveys are reasonably well approximated by $P(k) \propto k^{-1.5}$ at wavenumbers $k \gtrsim 0.1 \text{ h Mpc}^{-1}$ and there is no convincing evidence for a turn-over to a scale-invariant form, $P(k) \propto k$, at smaller wavenumbers. However, such a turn-over must exist since measurements of the microwave background fluctuations on angular scales $\gtrsim 1^\circ$ suggest a near scale-invariant spectrum of perturbations on spatial scales $\gtrsim 100 \text{ h}^{-1}\text{Mpc}$ (see the reviews by Scott, Silk & White 1995 and Bond 1996).

A convincing detection of a turn-over in the power spectrum of density irregularities is therefore of fundamental significance and would establish a direct link between fluctuations observed in the microwave background radiation and

those observed in the density distribution. Furthermore, in theories such as the Cold Dark Matter (CDM) model, a peak in the power spectrum is predicted on the scale of the Hubble radius at the time that matter and radiation have equal density, $\lambda_{equ} \sim 10(\Omega h^2)^{-1}\text{Mpc}$ (see e.g. Efstathiou 1990). An observation of a peak in the power spectrum of galaxy clustering can therefore be used to constrain the parameter $\Gamma = \Omega h$ that is fundamental to CDM models.

There is some tentative evidence for a turn-over at a wavenumber $k \sim 0.025$ in the three-dimensional power spectrum inferred from the two-dimensional clustering of galaxies measured from the APM galaxy survey (Baugh & Efstathiou 1993, Baugh & Efstathiou 1994, see for example Figure 11 of Baugh & Efstathiou 1994). Gaztanaga & Baugh (1997) have carefully investigated the significance of this observed turn-over by repeating, using simulations of the APM galaxy survey, the procedure of inverting the two-dimensional clustering statistics to obtain the three-dimensional power spectrum. They conclude that the turn-over, which occurs between $0.02 < k < 0.06 \text{ h Mpc}^{-1}$, can be reproduced by the inversion process. However, at these small wavenumbers, the systematic errors in the construc-

tion of the APM Galaxy Survey are difficult to quantify and could perhaps be greater than the random errors (see Maddox, Efstathiou & Sutherland 1996 for a detailed discussion of systematic errors in the APM survey). It is therefore difficult to assign a meaningful statistical significance to this result.

The detection of a peak in the power spectrum of the galaxy distribution is one of the main scientific goals of the Anglo-Australian 2dF redshift survey (see e.g. Efstathiou 1996) and the Sloan Digital Sky survey (Gunn & Weinberg 1995) which aim to measure redshifts of $\sim 10^6$ galaxies. However, in this paper we show that redshift surveys of much smaller numbers ($\sim 10^3$) of rich clusters of galaxies can provide accurate measurements of the power spectrum on large spatial scales. Relatively little work has been done on the three-dimensional power spectrum of rich clusters of galaxies (see Gramman & Einasto 1992, Peacock & West 1992, Einasto et al. 1993). Most recent work has focused on measurements of the two-point spatial correlation function of rich clusters of galaxies, $\xi(r)$, and whether systematic errors in the cluster catalogues affect the amplitude of $\xi(r)$ on scales $\lesssim 20 h^{-1}\text{Mpc}$. The closest investigation to the one presented here is that of Peacock and Nicholson (1991), who describe a power spectrum analysis of a redshift survey of 310 radio galaxies. Their results are described in further detail in Section 4.

In this paper we analyse the redshift survey of 364 APM clusters described by Dalton et al. (1994). In previous papers (Dalton et al. 1992, Dalton et al. 1994), we have applied a number of tests to show that the APM cluster catalogue is free of the projection and selection biases known to affect clustering in the Abell cluster catalogues (Sutherland 1988, Efstathiou et al. 1992). As we show here, the large volume surveyed by the APM cluster survey ($V \gtrsim 3 \times 10^7 h^{-3} \text{Mpc}^3$) renders it suitable for an investigation of clustering on very large scales.

This paper is laid out as follows. In Section 2 we summarize the techniques used in the power spectrum analysis. We apply these techniques to the APM cluster survey and investigate the sensitivity of our results to the selection function, weighting function and background cosmological model. In Section 3 we construct simulated APM cluster catalogues from large N-body simulations to quantify any systematic errors and biases in our power spectrum estimator. From this analysis we can assess the significance of the observed peak in power spectrum of APM clusters. Our conclusions are presented in Section 4.

2 ESTIMATION OF THE POWER SPECTRUM

The analysis described here is similar to the power spectrum analysis of the Stromlo-APM galaxy redshift survey described by Tadros & Efstathiou (1996) (hereafter TE96). We follow their notation unless otherwise stated. We apply the power spectrum analysis to the redshift survey of APM clusters described by Dalton et al. (1994). We use the largest statistically uniform sample of APM clusters, Sample B of Dalton et al. (1994) containing 364 clusters over the southern APM area ($21^h \lesssim RA \lesssim 5^h$, $-72.5^\circ \lesssim dec \lesssim -17.5^\circ$). The number density of clusters in this sample is $\sim 3.4 \times 10^{-5} (h^{-1}\text{Mpc})^{-3}$. The redshift distribution of the

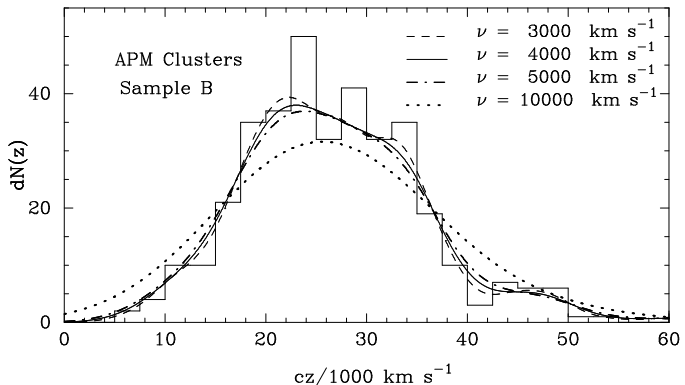


Figure 1. Histogram of the redshift distribution of the 364 clusters in Sample B of the APM cluster redshift survey. The lines show the result of smoothing the histogram with a Gaussian of width ν for four values in the range 3000 – 10000 km s^{-1} as indicated in the figure.

sample is shown in Figure 1. The median redshift of the sample is $z_{med} = 0.09$ and the cluster distribution extends to a redshift $z \sim 0.2$.

2.1 Method

We treat the APM cluster redshift survey in the same way as a flux limited galaxy survey, and use the methods of Feldman, Kaiser & Peacock (1994) (hereafter FKP), as implemented by TE96, to account for the radially varying selection function. To define the selection function of the survey we smooth the velocity distribution shown in Figure 1 with a Gaussian of width $\nu \text{ km s}^{-1}$. The fiducial value of ν is 4000 km s^{-1} .

The estimation of the power spectrum may be summarized as follows (for further details the reader is referred to TE96). We compute a weighted density field

$$F(\mathbf{r}) = \frac{w(\mathbf{r}) [n_c(\mathbf{r}) - \alpha n_s(\mathbf{r})]}{[\int \bar{n}^2(\mathbf{r}) w^2(\mathbf{r}) d^3r]^{\frac{1}{2}}}, \quad (1)$$

where the subscript c denotes the cluster density in the real catalogue and s denotes the density field for a random catalogue with same angular and radial selection functions as the cluster survey. In equation (1), $\bar{n}(\mathbf{r})$ is the expected mean density of clusters in a catalogue with the same angular and radial selection functions as the data. The radial selection function is derived from the fits to the redshift distribution plotted in Figure 1. The function $\bar{n}(\mathbf{r})$ can be separated into the mean galaxy density $\bar{n}(r)$ as a function of radial distance r , multiplied by the angular mask of the catalogue (*i.e.* the distribution of the APM galaxies on the sky defined by the survey boundary and excluding regions around bright stars, globular clusters *etc.*). The factor α is the ratio of the space densities in the real catalogue to that in the random catalogue. In the analysis presented here we use several thousand times as many points in the random catalogue as there are clusters in the real catalogue, and compute α from the ratio of the sums

$$\sum_i \frac{1}{(1 + 4\pi\bar{n}(r_i)J_3)}, \quad (2)$$

where we have set $4\pi J_3 = 40000(h^{-1}\text{Mpc})^3$ and the sums

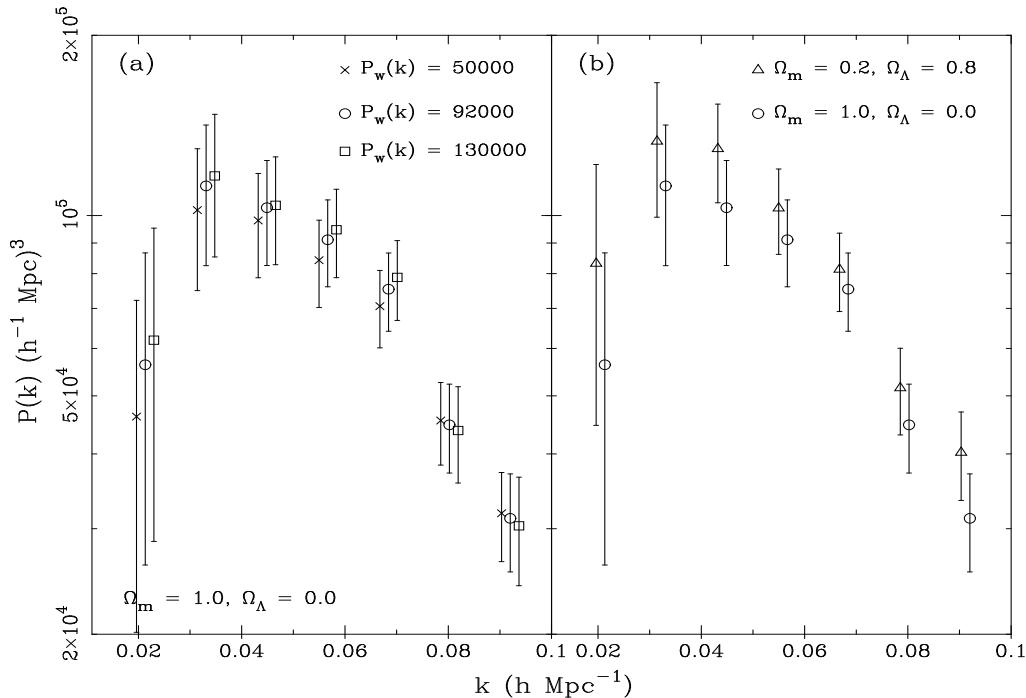


Figure 2. Three-dimensional power spectra of the APM clusters redshift survey. Panel (a) shows the effect of using different values of $P_w(k)$ in the weighting function of equation (3). Three values are used: $P_w(k) = 50000, 92000$ and $130000 (h^{-1} \text{Mpc})^3$ as shown by the crosses, circles, and squares respectively. The estimates in Panel (a) assume a spatially flat geometry with $\Omega_\Lambda = 0$. Panel (b) shows the effect of varying the assumed cosmology. The power spectrum is shown for two spatially flat models: $\Omega_m = 1.0, \Omega_\Lambda = 0.0$ (circles), and $\Omega_m = 0.2, \Omega_\Lambda = 0.8$ (triangles). Both spectra in the right hand panel have $P_w(k) = 92000 (h^{-1} \text{Mpc})^3$ in the weighting function. For clarity, sets of points have been offset from each other by one seventh of the bin spacing in both panels.

run over all clusters and random points (see Efstathiou 1996, Section 5.3 for details). The specific choice for J_3 is based on the power spectra of CDM models multiplied by a factor ~ 4 to account for the bias of clusters with respect to the underlying mass distribution. However, the results presented below are insensitive to the exact value of $4\pi J_3$ used in the analysis.

Each cluster in the analysis is weighted according to the minimum variance weight function (FKP)

$$w(r) = \frac{1}{1 + \bar{n}(r) P_w(k)}, \quad (3)$$

which depends on the value of $P_w(k)$ at each wavenumber k . We have set $P_w(k)$ in equation (3) equal to a constant value and investigated how the estimates of the power spectrum change for three values of $P_w(k)$: 50000, 92000 and 130,000 $(h^{-1} \text{Mpc})^3$, which span the range of the observed power spectrum over a wide range of wavenumbers. The power spectrum is derived by Fourier transforming equation (1), removing shot noise (equation 2.1.9 of FKP) and averaging the power-spectrum estimates over shells in k -space of volume V_k . The power spectrum estimates will be correlated over a range in k -space given approximately by $\delta k \sim D^{-1}$ where D is the characteristic depth of the survey. To obtain roughly independent points, all power spectra presented in this paper (except those calculated from the full periodic box of the N-body simulations described in Section 3) have been binned over a range in wavenumber $\sim D^{-1}$.

To perform the power spectrum analysis one must define a background cosmological model. Firstly, a cosmology must be assumed in the conversion of cluster redshifts to proper distances, and secondly a cosmological volume element must be used to obtain the radial number density from the solid line in Figure 1. Since the median redshift of clusters in the APM survey $z_{med} = 0.09$, the assumed cosmology may affect the results. Consequently we have carried out the analysis for two assumed cosmologies. Firstly a spatially flat universe with a matter density parameter $\Omega_m = 1.0$, and secondly a spatially flat universe with $\Omega_m = 0.2$, and a cosmological constant contributing most of the closure density, $\Omega_\Lambda = 0.8$. The results for an open universe with $\Omega_m = 0.2$ and $\Omega_\Lambda = 0$ are intermediate between those for the two spatially flat models.

2.2 Computation of Errors

Error bars on $P(k)$ are computed using equation (2.4.6) of Feldman, Kaiser & Peacock (1994). Their expression was derived assuming that the density field of the tracer objects followed a Gaussian distribution. This will not be true on small scales where the density fluctuations in the cluster distribution are greater than unity, even if the primordial fluctuations were strictly Gaussian. Thus, in Section 3.2 we test the accuracy of the error estimates using mock cluster catalogues generated from large N -body simulations.

2.3 Results for $P(k)$

In Figure 2 we show the power spectrum for the 364 clusters in the APM cluster redshift survey. The cluster sample was truncated at a proper distance of $r_{max} = 600 h^{-1}\text{Mpc}$ and the selection function for the sample was derived by smoothing the cluster redshift distribution with a Gaussian of width 4000km s^{-1} as illustrated in Figure 1.

Figure 2(a) shows the cluster power spectra calculated assuming values of $P_w(k) = 50000, 92000$ and $130,000 (h^{-1}\text{Mpc})^3$ in the weighting function (equation 3) and distances computed assuming a spatially flat universe with zero cosmological constant. Figure 2(b) shows the effect of changing the underlying cosmological model whilst keeping the weighting parameter fixed at $P_w(k) = 92,000 (h^{-1}\text{Mpc})^3$. The circles show the power spectrum derived assuming a spatially flat cosmology with $\Omega_m = 1.0, \Omega_\Lambda = 0$ and the triangles show the power spectrum calculated assuming $\Omega_m = 0.2, \Omega_\Lambda = 0.8$. This comparison shows that uncertainties in the background cosmological model can affect the amplitude of the cluster power spectrum by a factor of up to ~ 1.3 , but that the shape of the power spectrum is not significantly affected. Figure 2 shows that the power spectrum of APM clusters is well approximated by a power law $P(k) \propto k^n$ with index $n = -1.6 \pm 0.3$ over the wavenumber range $0.04 < k < 0.1 h \text{Mpc}^{-1}$. The power spectrum flattens at smaller wavenumbers and appears to turn-over a wavenumber $k \sim 0.03 h \text{Mpc}^{-1}$.

2.4 Sensitivity of $P(k)$ to weighting and selection function

Figure 2 shows that the power spectrum of APM clusters is not very sensitive to the value of $P_w(k)$ assumed in the weighting function of equation (3). Changing the weighting factor $P_w(k)$ by relatively large amounts leads to changes in the power spectrum points that are very much smaller than the error bars.

The power spectrum estimates are more sensitive to the value of ν , the velocity smoothing parameter that is used to generate a smooth selection function from the cluster redshift distribution (see Figure 1). Figure 3(a) shows power spectra calculated using three values for this smoothing, 3000km s^{-1} and 5000km s^{-1} (spanning the fiducial value of 4000km s^{-1} used in the estimates of Figure 2) and a much larger value, $\nu = 10000\text{km s}^{-1}$. For these estimates we use a constant weighting factor of $P_w(k) = 92000 (h^{-1}\text{Mpc})^3$. Although the power spectra are insensitive to the smoothing velocity for small changes around the fiducial value of 4000km s^{-1} , if we smooth with $\nu = 10,000\text{km s}^{-1}$ the amplitude of the power spectrum at wavenumbers $k \lesssim 0.035$ rises sufficiently to eliminate the turnover in $P(k)$. For the largest smoothing, the selection function is a poor fit to observed redshift distribution, and particularly to the small number of high redshift clusters ($z > 0.13$, see Figure 1). We find that the sensitivity of the power spectrum estimates to the selection function smoothing can be reduced substantially by truncating the sample at a proper distance of $r_{max} = 400 h^{-1}\text{Mpc}$, thus eliminating the high redshift tail of the cluster $n(z)$ distribution. This is illustrated in Figure 3(b) which shows $P(k)$ estimates for the same three

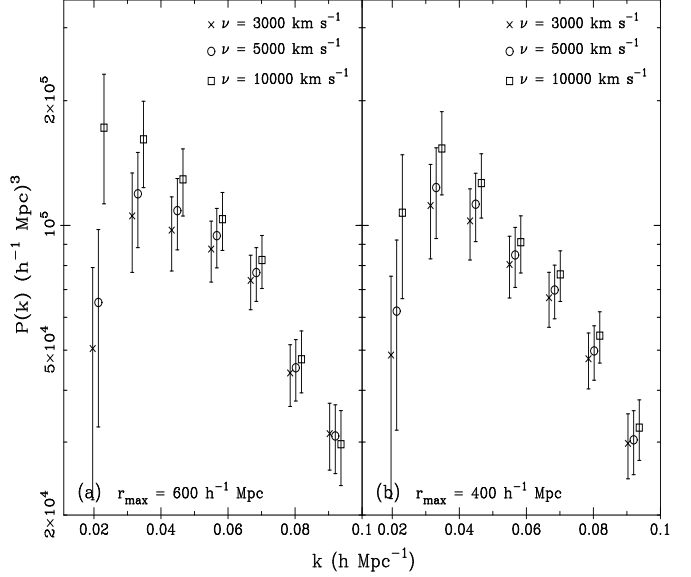


Figure 3. Figure 3(a) shows the effect on the power spectrum estimates of changing the value of ν used to smooth the cluster redshift histogram (see Figure 1). Estimates of $P(k)$ are shown for three values of ν : $\nu = 3000 \text{ km s}^{-1}$ (crosses), $\nu = 5000 \text{ km s}^{-1}$ (circles) and $\nu = 10000 \text{ km s}^{-1}$ (squares). The power spectrum becomes sensitive to the value of ν for wavenumbers $k \lesssim 0.035 h \text{Mpc}^{-1}$. Figure 3(b) is identical to Figure 3(a) except that we have limited the cluster sample to clusters with proper distances of less than $400 h^{-1}\text{Mpc}$. For all of these estimates, we have assumed a constant weighting factor of $P_w(k) = 92000 (h^{-1}\text{Mpc})^3$ and a spatially flat background cosmology with $\Lambda = 0$. For clarity, sets of points have been offset from each other by one seventh of the bin spacing in both panels.

velocity smoothings as in Figure 3(a) but where we have truncated the cluster sample at $r_{max} = 400 h^{-1}\text{Mpc}$. In this figure the three estimates of $P(k)$ are compatible to well within the 1σ error bars. The effect of the velocity smoothing is to produce a slight change in the amplitude of $P(k)$ and all three estimates show a turnover at $k \sim 0.03 h \text{Mpc}^{-1}$.

Unless otherwise stated, in the rest of this paper we will use the APM cluster power spectrum computed under following assumptions:

- (i) $P(k) = 92000 (h^{-1}\text{Mpc})^3$ in the weighting function of equation (3).
- (ii) A smoothing velocity $\nu = 4000 \text{ km s}^{-1}$ to define the selection function.
- (iii) $r_{max} = 400 h^{-1}\text{Mpc}$.
- (iv) A spatially flat background cosmology with zero cosmological constant.

To summarize, this section shows that the shape of the estimated power spectrum is insensitive to these assumptions to within the 1σ error bars. However, plausible variations of these assumptions can lead to a change in the overall amplitude of $P(k)$ by up to a factor of 1.5.

3 COMPARISON WITH SIMULATED APM CLUSTER SURVEYS

In this section we investigate the reliability of the power spectrum estimator described in Section 2.1. We measure $P(k)$ from mock APM cluster surveys extracted from large N-body simulations to determine the minimum wavenumber at which the true power spectrum can be recovered accurately. From this investigation, we can assess the significance of the turn-over seen in the power spectrum of APM clusters at a wavenumber of $k \sim 0.03 \text{ h Mpc}^{-1}$ (Figures 2 and 3).

3.1 Construction of simulated surveys

We have constructed mock APM cluster redshift surveys from N-body simulations of two cold dark matter (CDM) models. The methods for creating mock catalogue from the numerical simulations are described in more detail by Croft and Efstathiou (1994). The simulations consist of two ensembles of 9 simulations each containing 160^3 particles within a periodic computational box of length $\ell_b = 600 \text{ h}^{-1}\text{Mpc}$. They are similar to the simulations described in detail by Croft and Efstathiou (1994) but employ more particles within a larger computation box. (The simulations of Croft and Efstathiou use 100^3 particles within a box of size $\ell_b = 300 \text{ h}^{-1}\text{Mpc}$). The simulations were run with the particle-particle-particle-mesh (P^3M) code described by Efstathiou et al. (1985) and model gravitational clustering in a CDM dominated universe with scale invariant initial density fluctuations. The two ensembles are as follows: the standard CDM model (Davis et al. 1985), *i.e.* a spatially flat universe with $\Omega_0 = 1$ and $h = 0.5$ (the SCDM ensemble); a spatially flat low density CDM universe with $\Omega_0 = 0.2$, $h = 1.0$, and a cosmological constant contribution $\Omega_\Lambda = \Lambda/(3H_0^2) = (1 - \Omega_0) = 0.8$ (the LCDM ensemble). The initial power spectra of the models are generated from the fitting function

$$P(k) \propto \frac{k}{\left[1 + \left(ak + (bk)^{\frac{3}{2}} + (ck)^2\right)^\nu\right]^{\frac{2}{\nu}}}, \quad (4)$$

where $\nu = 1.13$, $a = (6.4/\Gamma) \text{ h}^{-1}\text{Mpc}$, $b = (3.0/\Gamma) \text{ h}^{-1}\text{Mpc}$ and $c = (1.7/\Gamma) \text{ h}^{-1}\text{Mpc}$. Equation (4) is a good approximation to the linear power spectrum of scale-invariant CDM models with low baryon density, $\Omega_b \ll \Omega_0$ (Bond & Efstathiou 1984). The parameter Γ in equation (4) is equal to $\Omega_0 h$. Thus $\Gamma = 0.5$ for the SCDM ensemble and $\Gamma = 0.2$ for the LCDM ensemble.

The final output times of the models are chosen to approximately match the microwave background anisotropies measured in the first year COBE maps (Smoot et al. 1992) ignoring any contribution from gravitational waves. Thus the *rms* mass fluctuations in spheres of radius $8 \text{ h}^{-1}\text{Mpc}$ are $\sigma_8 = 1$. The clustering statistics of clusters of galaxies are a very weak function of time, so the simulation output time used is not a critical consideration (see e.g. Croft & Efstathiou 1994).

Candidate cluster centres are selected by using a friends-of-friends algorithm to link particles with separation less than 0.1 times the mean inter-particle separation. These group centres are then used as the centres of spheres of size $r_c = 0.5 \text{ h}^{-1}\text{Mpc}$ within which the mass of the cluster is

calculated. The centre of mass of the cluster was found and any cluster which was less than r_c from the centre of another, richer cluster was deleted. The procedure was then repeated, and a final list of clusters was generated and ordered by mass. A lower mass cut off was applied to generate a cluster sample of a chosen mean number density.

The mock surveys extracted from the cluster distribution are designed to sample the same volume as the APM cluster survey using the same sky mask as the real data (*i.e.* the identical area of the sky and excluded areas such as holes around bright stars and globular clusters). The lower mass cut-off of clusters identified in the N-body simulations was adjusted to match the space-density of clusters in the real APM cluster redshift survey. The mock catalogues were limited at a proper distance of $600 \text{ h}^{-1}\text{Mpc}$; however we have checked that the results and conclusions of this section are unchanged if the mock catalogues are limited at the smaller distance of $400 \text{ h}^{-1}\text{Mpc}$. The smoothed APM cluster selection function ($\nu = 4000 \text{ km s}^{-1}$) was imposed on the cluster catalogues and (since the peculiar velocities of the clusters in the N-body simulations are known) we shifted the clusters to their redshift space positions to create mock APM catalogues in redshift space.

3.2 $P(k)$ from simulated surveys

Figure 4 shows the power spectra measured from the mock APM cluster catalogues, using the estimator described in Section 2. The crosses show the average value of $P(k)$ measured from 27 mock surveys for each ensemble using three randomly chosen centres for each simulation. The error bars show the standard deviation of the mean $P(k)$, computed from the scatter over the 27 mock surveys. The circles in Figure 4 show the mean redshift-space power spectrum for each ensemble computed from the full N-body simulation volume (*i.e.* with no application of a selection function or angular sky mask). The values of $P_w(k)$ used in the weighting function were $P_w(k) = 50000 \left(\text{h}^{-1}\text{Mpc}\right)^3$ and $P_w(k) = 16000 \left(\text{h}^{-1}\text{Mpc}\right)^3$ for the LCDM and SCDM simulations respectively. These values of $P_w(k)$ were chosen to provide a match to the mean amplitude of $P(k)$ from these two cosmological models over the range of wavenumbers plotted in the figure. The figure shows that our estimator of $P(k)$ based on equation (1) provides a good measure of the power spectrum of APM-like cluster catalogues in the LCDM model for wavenumbers $k \gtrsim 0.02 \text{ h Mpc}^{-1}$. For the SCDM model, we see some differences in the power spectra estimates at wavenumbers $0.02 - 0.05 \text{ h Mpc}^{-1}$, but these are not large enough to eliminate the break in the power spectrum estimates for the mock APM catalogues.

TE96 give a detailed analysis of biases in estimating the power spectrum from redshift surveys. There are two effects that can lead to systematic differences between the estimated and true power spectra on large scales: (a) the estimated power spectrum is a convolution of the true power spectrum and the power spectrum of the window function of the survey; (b) the estimated power spectrum is biased low at small wavenumbers if the mean space density of the sample is estimated from the survey itself. Both effects depend on the geometry of the survey and on the form of the true power spectrum and will affect the estimates of $P(k)$

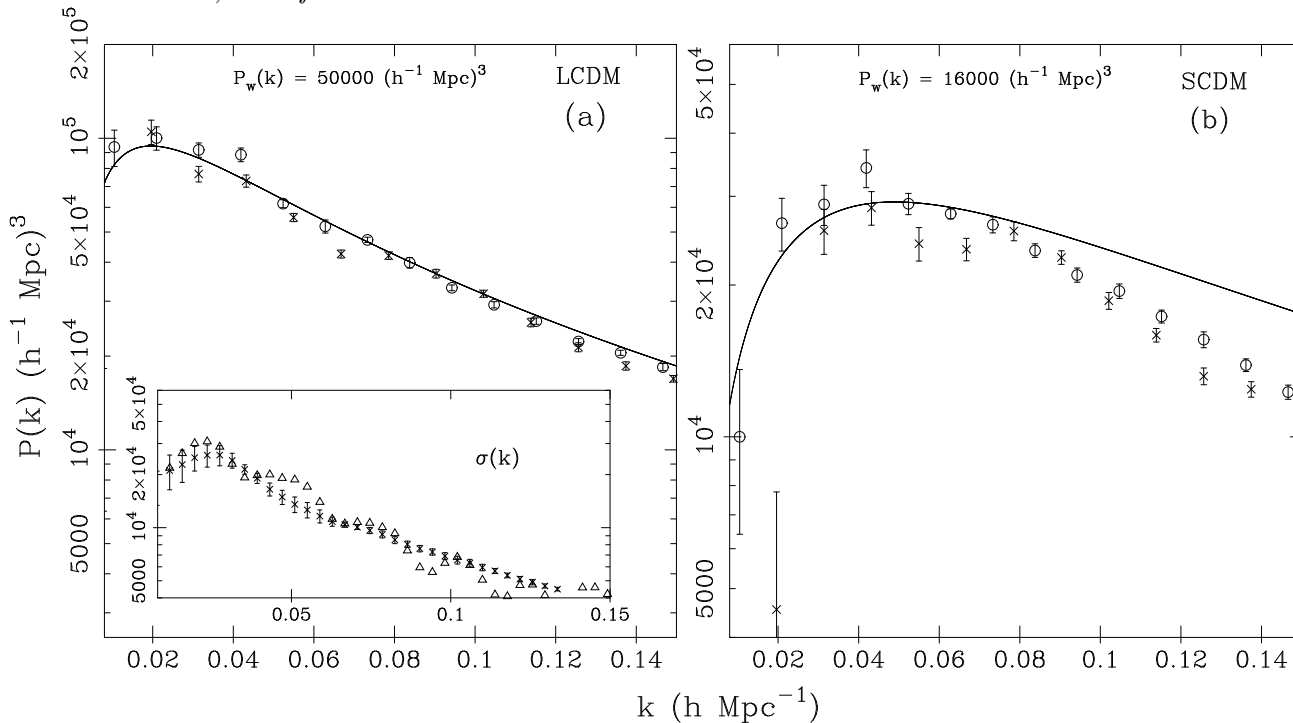


Figure 4. The circles plotted in each of the two panels show the redshift-space power spectrum of clusters in the LCDM model (left hand panel) and the SCDM model (right hand panel) computed from the full periodic volume of the N-body simulations. The crosses show the power spectra estimated from the average over 27 realizations of the APM cluster redshift survey constructed from the simulations. The error bars in all cases show the error on the mean value of $P(k)$. The power spectrum estimated from mock APM cluster catalogues is in good agreement with the power spectrum computed from the full simulation volumes on scales $k \geq 0.02 \text{ h Mpc}^{-1}$ for the LCDM model, and $k \geq 0.03 \text{ h Mpc}^{-1}$ for the SCDM model. The solid lines show the linear theory spectra for the two models normalized arbitrarily to match the data points at wavenumbers $k \sim 0.05 \text{ h Mpc}^{-1}$. The inset in the left hand panel shows the performance of the error estimator (equation 2.4.6 of FKP). The triangles in the inset plot show the error bar on the mean $P(k)$ obtained from the 27 realizations of the mock APM catalogues. The crosses show the error, $\sigma(k)$, derived by using equation (2.4.6) of FKP. The error bar plotted on each of the crosses shows the size of the error on the mean error, obtained from the spread in the measured $\sigma(k)$ over the 27 realizations of the APM cluster catalogue.

from the mock APM catalogues plotted in Figure 4. However, these biases are not present in the power spectrum estimates from the full periodic volumes of the N-body simulations (plotted as the circles in Figure 4). Thus, the close agreement between the power spectra in each of Figures 4(a) and 4(b) shows that neither bias is significant for wavenumbers $k \gtrsim 0.02 \text{ h Mpc}^{-1}$.

The inset in the left hand panel of Figure 4 shows a test of the error estimator used in this analysis. The crosses show the error bars calculated from equation (2.4.6) of FKP, averaged over 27 realizations. The errors on each of these points show the error on the mean. The triangles show the error on $P(k)$ calculated by evaluating the spread in the measured value of $P(k)$ over the 27 realizations of the APM cluster survey. Thus equation (2.4.6) of FKP provides an excellent estimate of the true error on $P(k)$ for all but the largest wavenumbers plotted in the figure.

In Figure 5 we compare the power spectrum of the APM clusters with the power spectra measured from the mock catalogues described above. The points for the real survey differ slightly in the two panels because in each case we assume background cosmologies consistent with the LCDM and SCDM theoretical models (*cf* Figure 2b). The APM cluster power spectrum cannot be matched by the SCDM model, in agreement with our previous analyses of the spatial two-point correlation function of the APM cluster sur-

vey (Dalton et al. 1992, Dalton et al. 1994). The LCDM model is much closer to the observations in shape and amplitude, but under-predicts the clustering strength and does not reproduce the turnover in the observed power spectrum at $k \lesssim 0.03 \text{ h Mpc}^{-1}$. A scale-invariant CDM model with a lower value of Γ ($\Gamma \approx 0.15$) would likely provide a better match to the clustering amplitude of rich clusters at wavenumbers $k \sim 0.04 \text{ h Mpc}^{-1}$ (e.g. see Figures 8 and 9 of Gaztanaga, Croft & Dalton 1995) but would fail even more strongly to match the downturn in the observed power spectrum at small wavenumbers.

These discrepancies between theory and observation do not seem particularly problematic, given the uncertainties in both the observational estimates and theoretical models. Neither the SCDM or LCDM models considered here provide an acceptable match to the observations, but these belong to a highly restricted class of CDM model. It may be possible to achieve a better match with a CDM-type model by allowing other parameters to vary, *e.g.* by incorporating a tilt in the primordial spectral index (White et al. 1995), or by invoking an admixture of hot and cold dark matter (Klypin et al. 1993).

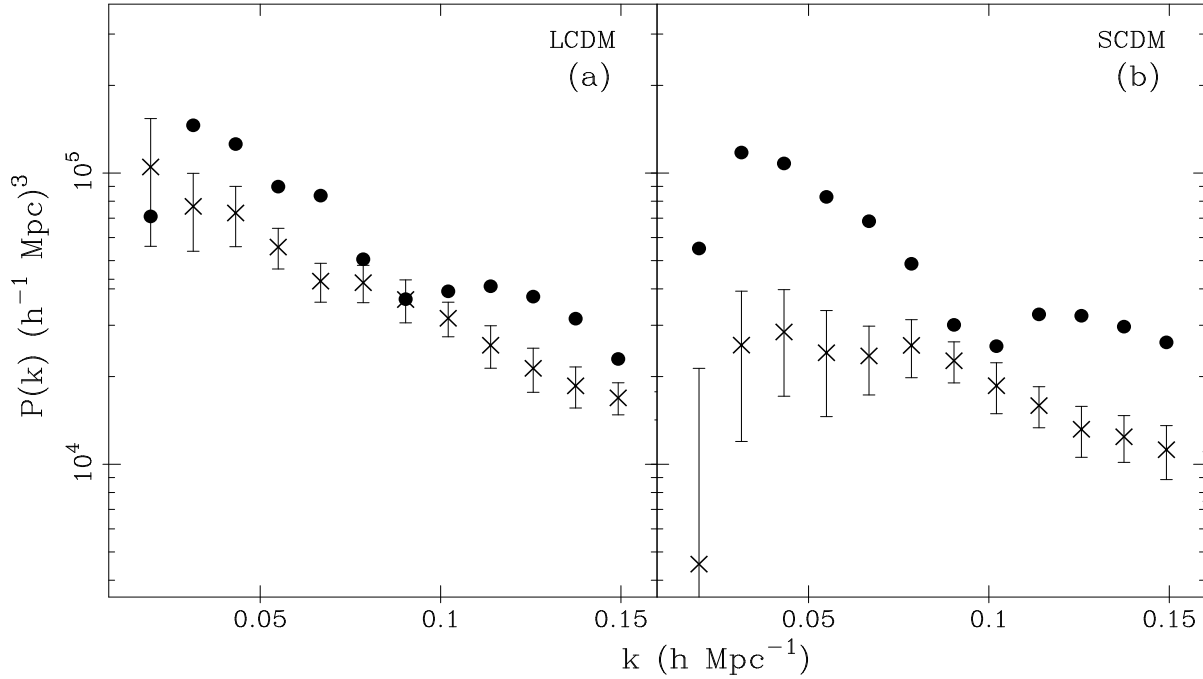


Figure 5. A comparison of the power spectrum of APM clusters with the predictions of the LCDM and SCDM models. The crosses in each case show the average power spectra of 27 mock APM cluster surveys extracted from the N-body simulations, together with 1σ errors appropriate to a single mock survey. The circles show the power spectra computed for the real APM cluster survey assuming a background cosmology that is consistent with the theoretical models.

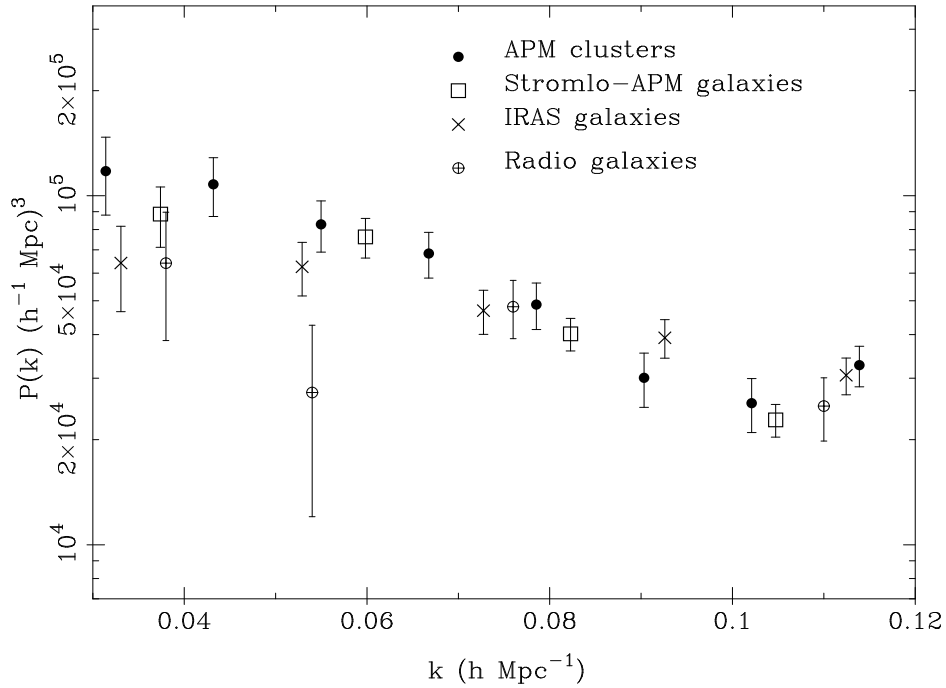


Figure 6. The power spectrum of APM clusters together with that of IRAS galaxies, optical galaxies and radio galaxies. The galaxy power spectra have been scaled upward by a scale-independent factor (see Table 1) to match the amplitude of the APM cluster power spectrum.

Table I

	k h Mpc $^{-1}$	b_c^2	$\chi^2/d.o.f$	P
IRAS	0.05 - 0.1	6.43 ± 0.73	1.65	0.18
Stromlo-APM	0.05 - 0.1	3.13 ± 0.32	0.19	0.90
Radio gals	0.04 - 0.1	0.99 ± 0.15	1.34	0.25

Table 1. Values for the relative bias (squared) between IRAS, optical and radio galaxies compared to APM clusters. Column 2 gives the range in wavenumber over which the fit was performed. Column 3 gives the factor by which the galaxy power spectrum must be scaled to match the clusters power spectrum i.e. the relative bias squared. The last two columns give the χ^2 per degree of freedom and the probability for the fit to a scale-independent relative bias.

4 DISCUSSION

We first compare the power spectrum of rich clusters with those for other types of object in the Universe. Figure 6 shows the APM cluster power spectrum together with power spectra for optical Stromlo-APM galaxies (Loveday et al. 1992a, TE96), IRAS galaxies (from the combined QDOT and 1.2Jy surveys, as calculated in Tadros & Efstathiou 1995) and a sample of 310 radio galaxies (as calculated by Peacock & Nicholson 1991). The spectra for optical, radio and IRAS galaxies have been scaled upwards by constant factors b_c^2 to match the amplitude of the APM clusters power spectrum. The factors b_c are thus the relative bias parameters for the three samples and are computed by performing a weighted fit to the ratio of the observed power spectra over a specified range in wavenumber. Table 1 lists the range in wavenumber over which the data were fitted, the values of the relative bias factors b_c , as well as the probability for the fit. A reasonable value for the fit probability shows that these power spectra are consistent with the hypothesis of a linear relative bias between the various tracer objects over the scales indicated in Table 1.

Peacock & Dodds (1994) found a relative bias parameter of 2.37 between radio galaxies and Abell clusters. This differs from the lower relative bias between radio galaxies and APM clusters listed in Table 1. This is a result of the higher amplitude of the power spectrum of Abell compared to APM clusters. However, there is now a large body of evidence to show that the clustering of Abell clusters is enhanced by non-uniformities in the Abell catalogue and does not reflect the true clustering properties of rich clusters (Sutherland 1988, Efstathiou et al. 1992, Croft et al. 1997). The relative bias of $b_c = 0.99$ between radio galaxies and APM clusters from Table 1 is thus consistent with the idea that luminous radio galaxies preferentially inhabit the cores of rich clusters of galaxies.

The agreement between the shapes of the power spectra for rich clusters of galaxies, IRAS and optically selected galaxies is consistent with a simple linear bias model. This provides an argument against models in which the galaxy formation process introduces spatial correlations so that galaxies are non-linearly biased with respect to the mass distribution (see *e.g.* Babul & White 1991). Figure 6 suggests a simpler interpretation, in which different types of galaxies and rich clusters are linearly biased on large-scales and each traces the shape of the underlying matter power spectrum.

We have found some evidence from the power spectrum of the APM cluster sample for a peak at $k \sim 0.03$ h Mpc $^{-1}$,

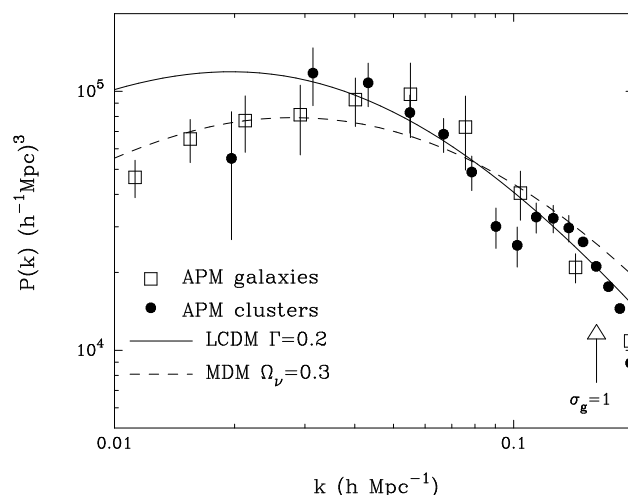


Figure 7. The filled circles show the power spectrum of APM clusters as plotted in Figure 6. The open squares show the power spectrum of APM galaxies estimated by inverting the two-dimension angular correlation function as described by Maddox et al. 1996 (see their Figures 32 – 35). The APM galaxy power spectrum has been multiplied by a factor of 5 to match the amplitude of the cluster power spectrum. The error bars were determined from the scatter in the inversions from four nearly equal area zones of the APM survey. The two lines show linear theory power spectra for a scale-invariant LCDM model with $\Omega_\Lambda = 0.8$, $h = 1$ (solid line) and a mixed dark matter model with $\Omega_\nu = 0.3$, $h = 0.5$. The linear spectra have been normalised arbitrarily to match the cluster power spectrum approximately in the region $k \sim 0.05$ h Mpc $^{-1}$.

followed by a downturn at smaller wavenumbers. The tests described in Section 3 suggest that the biases in the estimator of $P(k)$ are too small to cause such a downturn. Figure 7 shows the APM cluster power spectrum (filled circles) together with the three-dimensional power spectrum determined by inverting the angular two-point correlation function measured for the APM Galaxy Survey (open squares). The latter points are from the analysis of Maddox *et al.* (1996) who applied the inversion technique developed by Baugh and Efstathiou (1993). The amplitude of the APM galaxy power spectrum has been multiplied by a factor of 5 to match the amplitude of the cluster power spectrum. Both the cluster and galaxy power spectra show a peak at a wavenumber ~ 0.03 – 0.04 h Mpc $^{-1}$, which suggests that the peaks reflect a real feature of the underlying mass distribu-

tion. As mentioned in the introduction, such a peak must exist at a wavenumber $\gtrsim 0.01 \text{ h Mpc}^{-1}$ since the anisotropies of the cosmic microwave background radiation on angular scales $\gtrsim 1^\circ$ are well approximated by a scale-invariant initial spectrum (Bond 1996).

The lines in Figure 7 show linear theory power spectra for two models, normalized to match the observations at a wavenumber $k \sim 0.05 \text{ h Mpc}^{-1}$. The $\Gamma = 0.2$ LCDM model has too much power on large scales to provide a good match to either the cluster or galaxy power spectra. The dashed line shows a scale-invariant mixed dark matter (MDM) power spectrum, with parameters $\Omega_\nu = 0.3$, $\Omega_b = 0.05$, $\Omega_m = 0.65$, and $h = 0.5$ (where Ω_ν , Ω_b and Ω_m are the respective cosmological densities in massive neutrinos, baryons and cold dark matter). The power spectrum of the MDM model is computed from the fits given in Ma (1996), but over the range of wavenumbers plotted in Figure 7 there is little difference between the MDM spectrum and a CDM spectrum of the form (4) with $\Gamma = \Omega_m h \sim 0.3$. As Figure 7 shows, a CDM-like model with $\Gamma \sim 0.3$ has a peak in the power spectrum that approximately matches the observations.

Because of the low space density of rich clusters of galaxies and their enhanced clustering strength compared to normal galaxies, rich clusters provide a powerful probe of large-scale structure in the Universe. At wavenumbers $k \gtrsim 0.01 \text{ h Mpc}^{-1}$, redshift surveys of only a few thousand rich clusters are capable of providing comparable results on the power spectrum, to those from redshift surveys of order 10^6 galaxies. Figure 7 thus suggests that a modest increase in the size of the cluster redshift sample could confirm the reality of a peak in the power spectrum at a high significance level.

Acknowledgments: We thank John Peacock for communicating the power spectrum of radio galaxies in a machine readable form.

References

- Babul A., White S. D. M., 1991, MNRAS, 253, 31P
 Baugh C. M., Efstathiou G., 1993, MNRAS, 265, 145
 Baugh C. M., Efstathiou G., 1994, MNRAS, 267, 323
 Bond J. R., Efstathiou G., 1984, ApJ, 285, L45
 Bond J. R., 1996, in Schaeffer R., ed, *Cosmology and Large Scale, Les Houches Session LX*, August 1993. Elsevier Science Press
 Croft R. A. C., Efstathiou G., 1994, MNRAS, 267, 390
 Croft R. A. C., Dalton G. B., Efstathiou G., Maddox S. J., Sutherland W. J., 1997, MNRAS, *in press*
 Dalton G. B., Efstathiou G., Maddox S. J., Sutherland W. J., 1992, ApJ, 390, L1
 Dalton G. B., Croft R. A. C., Efstathiou G., Sutherland W. J., Maddox S. J., Davis M., 1994, MNRAS, 271, 47P
 Davis M., Efstathiou G., Frenk C. S., White S. D. M., 1985, ApJ, 292, 371
 Efstathiou G., Davis M., Frenk C. S., White S. D. M., 1985, ApJS, 57, 241
 Efstathiou G., Dalton G. B., Sutherland W. J., Maddox S. J., 1992, MNRAS, 257, 125
 Efstathiou G., 1990, in Peacock J. A., Heavens A. F., Davies A. T., eds, *Physics of the Early Universe*. S. U. S. S. P., p. 361
 Efstathiou G., 1996, in Schaeffer R., ed, *Cosmology and Large Scale, Les Houches Session LX*, August 1993. Elsevier Science Press
 Einasto J., Gramman M., Saar E., Tago E., 1993, MNRAS, 260, 705
 Feldman H. A., Kaiser N., Peacock J. A., 1994, ApJ, 426, 23
 Gaztanaga E., Baugh C. M., 1997, *preprint astro-ph/9704246*
 Gaztanaga E., Croft R. A. C., Dalton G. B., 1995, MNRAS, 276, 336
 Gramman M., Einasto J., 1992, MNRAS, 254, 453
 Gunn J. E., Weinberg D. H., 1995, in Maddox S. J., Aragon-Salamanca A., eds, *Wide Field Spectroscopy and the Distant Universe, The 35th Herstmonceux Conference*
 Klypin A., Holtzman J., Primack J., Regos E., 1993, ApJ, 416, 1
 Loveday J., Efstathiou G., Peterson B. A., Maddox S. J., 1992a, ApJ, 400, L43
 Ma C.-P., 1996, ApJ, 471, 13
 Maddox S. J., Efstathiou G., Sutherland W. J., 1996, MNRAS, 283, 1227
 Peacock J. A., Dodds S. J., 1994, MNRAS, 267, 1020
 Peacock J. A., Nicholson D., 1991, MNRAS, 253, 307
 Peacock J. A., West M. J., 1992, MNRAS, 259, 494
 Scott D., Silk J., White M., 1995, Sci, 268, 829
 Smoot G. F. et al., 1992, ApJ, 396, L1
 Sutherland W. J., 1988, MNRAS, 234, 159
 Tadros H., Efstathiou G., 1995, MNRAS, 276, 45P
 Tadros H., Efstathiou G., 1996, MNRAS, 282, 1381
 White M., Scott D., Silk J., Davis M., 1995, MNRAS, 276, 69P